Extended model for the interaction of dielectric thin films with an electrostatic force microscope probe

M. Labardi,[1,a)] J. Barsotti,[2,b)] D. Prevosto,[1] S. Capaccioli,[1,2] C. M. Roland,[3] and R. Casalini[3]
[1]*CNR-IPCF, UOS Pisa, Largo Pontecorvo 3, I-56127 Pisa, Italy*
[2]*Physics Department, University of Pisa, Largo Pontecorvo 3, I-56127 Pisa, Italy*
[3]*Chemistry Division, Naval Research Laboratory, Washington, D.C., USA 20375-5342*

(Received 25 September 2015; accepted 21 November 2015; published online 14 December 2015)

To improve measurements of the dielectric permittivity of nanometric portions by means of Local Dielectric Spectroscopy (LDS), we introduce an extension to current analytical models for the interpretation of the interaction between the probe tip of an electrostatic force microscope (EFM) and a thin dielectric film covering a conducting substrate. Using the proposed models, we show how more accurate values for the dielectric constant can be obtained from single-frequency measurements at various probe/substrate distances, not limited to a few tip radii. © *2015 AIP Publishing LLC*.
[http://dx.doi.org/10.1063/1.4937136]

INTRODUCTION

The demand for electronic device miniaturization and the employment of nanostructured materials tailored to achieve diverse mechanic, electronic, optoelectronic, or magnetic properties[1] motivate the development of electric characterization tools capable of probing nanometer sized volumes of conducting, semiconducting, and even insulating materials, for example, oxide layers or dielectrics in nanocapacitors.[2] These studies can be performed by scanning probe techniques like electrostatic force microscopy (EFM), where a sharp conducting tip of an atomic force microscope (AFM) is used essentially as a local electrostatic sensor,[3] being routinely capable of lateral resolution of 20–30 nm (see, e.g., Ref. 4). Along with efforts to improve such resolution down to the sub-10 nm level,[5] there is the need for more quantitative measurements that address spreading resistance,[6] contact potential,[7] or the dielectric constant.[8] Current analytical models describing the EFM signals for dielectric layers deposited on metallic substrates are limited to substrate/tip distances smaller than the apical radius of the tip.[9,10] However, for dielectric films much thicker than the apex radius, as well as operation with open-loop distance feedback such as lift-mode™,[11] it is not easy or even possible to perform measurements within such limits. Moreover, to obtain quantitative determination of the dielectric constant, it is necessary to measure electrostatic interaction at various tip/sample distances,[8] which is not easy from the experimental point of view, especially when substrate/tip distances must be kept below the apex radius, or when using tips with very small radii. For the above practical reasons, modeling of electrostatic interactions at tip/sample distance larger than several tip radii is required. Notwithstanding such difficulties, quantitative measurements of the dielectric constant in oxide layers or polymer films based on scanning probe techniques have been performed over the past few years. Some examples are measurements of nanoscale impedance[8] and electrostatic force microscopy.[9,12,13]

The most accurate way to describe electrostatic tip/sample interaction, and hence the capacitance, of realistic scanning probe systems is by numerical modeling;[9,13] however, this method is quite complex, time consuming, and not suitable for fitting multiple datasets, like distance-dependent signals or dielectric spectra. In particular, by local dielectric spectroscopy (LDS),[14] a scanning probe spectroscopic technique based on EFM, the frequency dependence of the dielectric relaxation function $\varepsilon^*(\Omega)$ of ultrathin polymer films can be determined, and a number of relaxation processes in glass forming systems can be characterized.[14–16] Even though the determination of the dynamics can be quantitative and accurate with this technique, to the best of our knowledge there are no reports of reliable absolute values for the dielectric function from LDS or other EFM techniques by using analytical models.

In this work, after providing a general description of the principles of EFM measurements, we present an overview of current EFM analytical models for the case of dielectric thin films, and propose an extended model that better describes EFM and LDS results over a wider tip/substrate distance range. The model has been validated on an ultrathin film of poly(vinyl acetate) (PVAc), allowing measurement of its dielectric constant with improved accuracy.

GENERAL GROUNDS

To understand the basic principles of LDS, it is useful to compare it to a standard technique for the electrical characterization of materials, namely, impedance or dielectric spectroscopy.[17] In dielectric spectroscopy, generally a thin sheet of the material under study is contained between two metal plates, forming a parallel plate capacitor. In the approximation that the electric field is homogeneous inside the assembly and that border effects can be neglected, the complex

[a)]Author to whom correspondence should be addressed. Electronic mail: labardi@df.unipi.it.
[b)]Presently at Center for Micro-BioRobotics, Istituto Italiano di Tecnologia, and The Biorobotics Institute, Scuola Superiore Sant'Anna, Viale Rinaldo Piaggio 34, 56025 Pontedera, Italy.

capacitance $C^*(\Omega)$ at angular frequency Ω depends on the dielectric function $\varepsilon^*(\Omega)$ of the material, as

$$C^*(\Omega) = \varepsilon^*(\Omega) C_0, \tag{1}$$

where C_0 is the capacitance of empty capacitor having the same geometry

$$C_0 = \varepsilon_0 A/d, \tag{2}$$

with ε_0 the permittivity of vacuum and A the electrode area having a spacing d. If one were to measure the dielectric function of a small portion of the sample, one of the capacitor plates could be made smaller to reduce the area of the applied electric field. The resulting impedance would therefore increase, and the measured current would decrease below the noise level of most ultralow noise preamplifiers; this makes such measurements a challenging task.[8] Furthermore, when the size of the plate becomes comparable to the sample thickness, the assumption of a homogeneous field with negligible border effects is no longer valid, and Eq. (2) cannot be used to determine C_0 and thus $\varepsilon^*(\Omega)$.

In the case of electrostatic force microscopy, the conducting AFM tip is maintained at a controlled distance from a conducting substrate (Fig. 1), on which the dielectric layer is deposited. The tip is supported on a flexible cantilever that serves as the force sensor; detection of forces or their gradients are used to both determine the tip/surface distance (topographic measurement) and to measure electrostatic interactions in the lift mode. The dynamic cantilever behavior is customarily described by a simple harmonic oscillator, with spring constant k and resonant frequency f_0. The tip/sample system forms a capacitor with a small electrode area, whose geometry is different from simple parallel plates. Instead, the tip geometry can be described as a cone with a spherical apex, the latter being the part closest to the dielectric layer (Fig. 1). The difficulty of measuring a small current is overcome in EFM by measuring instead the electrostatic force between the two electrodes. This electrostatic force can be determined precisely and is related to the electric impedance through the electrostatic energy U_{el} stored in a capacitor C. In the case of a grounded substrate[7] with potential V applied to the tip, we have

$$U_{el} = \frac{1}{2} C V^2, \tag{3}$$

with the force in the parallel direction z in the case of a conserved potential V,[7] is given by

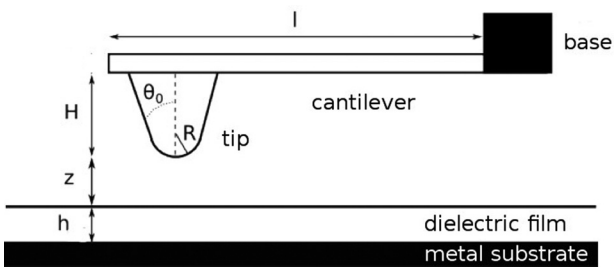

FIG. 1. Sketch of the tip/sample system geometry (not to scale).

$$F_z = \frac{1}{2} \frac{dC}{dz} V^2. \tag{4}$$

The most sensitive and high-resolution local measurements obtained in AFM are by detecting the force gradient in the approach direction dF_z/dz.[18] In fact, in spite of a lower signal-to-noise ratio, force gradients are more readily detectable, since they are proportional to the shift of the system resonant frequency Δf_{res} as

$$\Delta f_{res} = -\frac{f_0}{2k} \frac{dF_z}{dz}, \tag{5}$$

valid in the limit that oscillation amplitude is much smaller than the characteristic decay length of the interaction at hand.

The force gradient mode is also recognized to be the main route for higher spatial resolution EFM[19] and Kelvin probe force microscopy (KPFM).[5] In essence, the higher the derivative order, the smaller the volume of material close to the tip that can influence the measurement. This is a general trend in scanning probe microscopy that finds application as well in near-field optical microscopy.[20,21]

The main problem in extracting the value of the dielectric constant from force or force gradient measurements is modelling the tip/sample/substrate interaction (and hence of the system capacitance) for the relevant range of distances. In principle, a reliable way to carry out such capacitance is by numerical calculations;[9,13] however, these are time consuming, and cannot easily be used, for instance, for simultaneous determination of the dielectric constant at many different frequencies. An example in which an analytical model is desirable is the case of LDS applied to study dielectric relaxation processes, and analyze local dielectric spectra with proper relaxation functions, to thereby extract the relaxation time and shape parameters. This was carried out in recent investigations of confinement and interfacial effects on polymer dynamics.[4,14,15,22,23] In the following, we present an extended analytical model for EFM tip/sample/substrate interaction with a wider range of applicability than previously adopted models.

EFM MODELS

A convenient and well accepted model to describe the electrostatic interaction between a flat metal surface and a conical metal tip with spherical apex is due to Hudlet *et al.*[24] A variation for a parabolic apex that also takes into account the effect of the cantilever was proposed by Colchero *et al.*[19] Both models lead to analytical expressions for the electrostatic force, F, along z, valid under a number of approximations. We consider first the following expressions from Ref. 24

$$F_H^a = -\pi \varepsilon_0 R V^2 \left[\frac{1}{z} - \frac{1}{z + R(1 - \sin\theta_0)} \right], \tag{6a}$$

$$F_H^c = -\frac{\pi \varepsilon_0 V^2 \sin^2\theta_0}{(\pi/2 - \theta_0)^2} \left[\ln \frac{H}{z + R(1 - \sin\theta_0)} - 1 + \frac{R\cos^2\theta_0 / \sin\theta_0}{z + R(1 - \sin\theta_0)} \right], \tag{6b}$$

$F_H{}^a$ and $F_H{}^c$ are the two components of the force due, respectively, to the spherical apex and cone terms,[24] where R is the spherical apex radius, θ_0 the cone half-angle, and H the cone height.[25] This expression is obtained by integration over the tip surface of the electric force along z acting on the surface charge located on the tip.

In the case of Colchero's model (Ref. 19), the same approach is used, but the above integration is performed on the substrate surface instead of the tip. By adapting the calculations of the cone term in Ref. 19 to the case of a spherical tip in Ref. 24, the following expression is obtained:

$$F_C^c = -\frac{\pi\varepsilon_0 V^2}{(\pi/2-\theta_0)^2}\left[\ln\left(\frac{H}{z+R(1-\sin\theta_0)}\right) + \sin\theta_0\left(-1+\frac{R\cos^2\theta_0/\sin\theta_0}{z+R(1-\sin\theta_0)}\right)\right]. \quad (7)$$

Since the spherical apex term was not adopted in Ref. 19, its expression is not available therein; thus, we assume the same apex term of Ref. 24, i.e., $F_C{}^a = F_H{}^a$. However, the two cone contribution terms (Eqs. (6b) and (7)) calculated by integration for the tip or substrate surfaces are different, so the same should hold in principle for the two apex terms if calculated for the tip or substrate surfaces, since the calculation method is the same. This fact has the crucial implication that the total electric force acting on the tip or substrate is not equal and opposite, as would be required by Newton's third law. This is a consequence of the limitation due to approximations used in the models.

The effect of a dielectric layer covering the metal substrate was evaluated by Sacha *et al.*[9] using numerical calculations. In a short distance range $z \ll R$, the addition of a dielectric layer of thickness $h \ll R(1-\sin\theta_0)$ was found to be well described by the expression of the force F_M valid for the bare metal, modified with an effective distance $z+h/\varepsilon$, so that

$$F_M = \left(\frac{1}{2}C'_{\text{stray}} - \frac{\pi\varepsilon_0 R}{z+h/\varepsilon}\right)V^2, \quad (8)$$

where C'_{stray} is a constant describing the contribution to the force from farther parts of the probe (basically, the cone and cantilever). By similar arguments, Gomila *et al.*[10] proposed a generalization of the apex term of Eq. (6a) to the case of dielectric films, extending the distance validity range to $z+h/\varepsilon \approx R$. The related force expression is

$$F_G = -\pi\varepsilon_0 R V^2\left[\frac{1}{z+h/\varepsilon} - \frac{1}{z+h/\varepsilon+R(1-\sin\theta_0)}\right]. \quad (9)$$

It can be observed that the latter expression reduces to Sacha's expression for $\theta_0 = 0$ and $z+h/\varepsilon \ll R$, apart from the C'_{stray} constant term. The range of distance of the expression of Gomila was validated by comparison with numerical simulations,[10] and is also confirmed by the present work. However, experimental results reported herein confirm that these models are not always adequate to describe the effect of dielectric films, for instance, when $z+h/\varepsilon$ is not very small compared to the apex radius or when the dielectric film thickness becomes too large. The former condition is instead likely whenever higher spatial resolution is pursued, since in such a case smaller tip radii have to be employed. Also, when measurements of the distance dependence are required, the model can only be applied up to a limited distance. Accordingly, the introduction of a cone term is necessary, with the contribution of the cantilever also being considered;[19,26] this is mainly the case for force mode, but even for force gradient mode,[19] as we show below. As an illustration of this issue, Fig. 2 shows an example of the distance dependence of the tip apex and cone contributions to the electrostatic force gradient for a metal tip and a metal surface system, calculated using Hudlet's model for typical experimental conditions. For distances less than the tip radius R, the contribution of the apex clearly dominates, but a sensible contribution from the cone starts at $z \approx R$, equaling that from the apex at $z \approx 3R$, and becoming dominant at larger distances. Thus, the contribution of the cone can be approximated with a constant only at very small distances ($z \ll R$), while for larger distances, its dependence on z needs to be taken into account.

For frequency modulation methods, the relevant quantity that determines the frequency shift Δf is not the force but its gradient (Eq. (5)). Using the expression for the electrostatic force due to Gomila *et al.*,[10] for the case of a dielectric film we obtain for the frequency shift (Eqs. (5) and (9))

$$\frac{\Delta f_G}{V^2} = -\frac{f_0}{2k}\pi\varepsilon_0 R\left[\frac{1}{(z+h/\varepsilon)^2} - \frac{1}{[z+h/\varepsilon+R(1-\sin\theta_0)]^2}\right]. \quad (10)$$

Starting from the approach of Hudlet,[24] which takes into account the term due to the cone, we can describe empirically the electrostatic force for a dielectric film in a similar way, by replacing z with $z+h/\varepsilon$ in both Hudlet's expressions (Eqs. (6a) and (6b)) to obtain for the apex the same expression as Gomila (Eq. (10)), and for the cone

$$F_{EH}^c = -\frac{\pi\varepsilon_0 V^2\sin^2\theta_0}{(\pi/2-\theta_0)^2}\left[\ln\frac{H}{z+h/\varepsilon+R(1-\sin\theta_0)} - 1 + \frac{R\cos^2\theta_0/\sin\theta_0}{z+h/\varepsilon+R(1-\sin\theta_0)}\right], \quad (11)$$

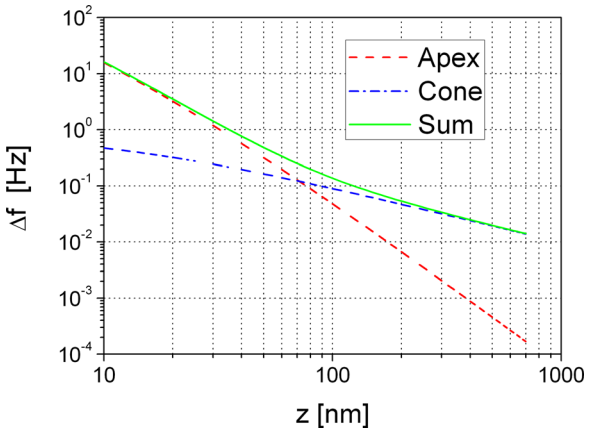

FIG. 2. Distance dependence of the frequency shift induced by a flat metallic surface on an AFM probe composed of a hemispherical apex on a truncated cone tip, calculated using the Hudlet model (Eqs. (6a) and (6b)), with $R = 20$ nm, $\theta_0 = 0.3$ rad, and $k = 2$ N/m.

where the subscript E indicates the extension to the dielectric layer case. The cone term, as in Eq. (11), is proposed for the first time.

Using Eqs. (5), (9), and (11), we can then derive the following expression for the frequency shift for a dielectric film

$$\frac{\Delta f_{\mathrm{EH}}}{V^2} = -\frac{f_0}{2k}\pi\varepsilon_0\left[\frac{R}{(z+h/\varepsilon)^2} - \frac{R\left[1-\cos^2\theta_0 \sin\theta_0/(\pi/2-\theta_0)^2\right]}{\left[z+h/\varepsilon+R(1-\sin\theta_0)\right]^2} + \frac{\sin^2\theta_0}{(\pi/2-\theta_0)^2}\frac{1}{\left[z+h/\varepsilon+R(1-\sin\theta_0)\right]}\right]. \quad (12)$$

This new expression, which is basically an "extended" Hudlet model, although formally more complicated than Gomila's model considering only the apex (Eq. (9)), actually depends on the same parameter set.

The same extension can be readily applied to the model of Colchero,[19] using Eqs. (5), (9), and (7)

$$\frac{\Delta f_{\mathrm{EC}}}{V^2} = -\frac{f_0}{2k}\pi\varepsilon_0\left[\frac{R}{(z+h/\varepsilon)^2} - \frac{R\left[1-\cos^2\theta_0/(\pi/2-\theta_0)^2\right]}{\left[z+h/\varepsilon+R(1-\sin\theta_0)\right]^2} + \frac{1}{(\pi/2-\theta_0)^2}\frac{1}{\left[z+h/\varepsilon+R(1-\sin\theta_0)\right]}\right]. \quad (13)$$

Motivated by the requirements of the action-reaction principle, we also derived an alternative model, similar to those above, but based on a different assumption for the evaluation of the electric field acting on the elementary surface charge. Instead of a dihedral approximation, where a circular field line is assumed to connect the two elementary surfaces on the tip dA_{T} and substrate dA_{S} (Fig. 3(a)),[19,24] a parallel plate approximation is used, with the tip surface decomposed into horizontal rings, lying in the plane orthogonal to z, whose area dA_{TP} corresponds to the projection of dA_{T} on the horizontal plane (Fig. 3(b)), and with the corresponding one on the substrate, dA_{SP}, obtained by projecting the ring onto the substrate surface. This model has the following implications: (i) since the resulting field lines are along z and the top and bottom areas are equal, integration on either tip or substrate of the z-force yields the same value; and (ii) addition of a dielectric layer exactly results in a reduction of the electric field complying with the replacement of z with $z+h/\varepsilon$. The main drawback of this "Straight" model is that the continuous tip shape is replaced by a large number of disconnected concentric rings, similarly to that shown in Ref. 27 for the modeling the cone contribution made therein. We have modeled the full tip (apex and cone) in this way, and found that the apex term can be integrated exactly, unlike in Refs. 19 and 24 where assumptions were needed to express the apex terms in a treatable way. The resulting expressions for our model are

$$F_S^a = -\pi\varepsilon_0 R V^2\left[\frac{1}{z} - \frac{1}{z+R(1-\sin\theta_0)} - \frac{1}{R}\ln\left(\frac{z+R(1-\sin\theta_0)}{z}\right)\right], \quad (14a)$$

$$F_S^c = -\pi\varepsilon_0 V^2 \tan^2\theta_0\left[\ln\left(\frac{H}{z+R(1-\sin\theta_0)}\right) - 1 + \frac{R\cos^2\theta_0/\sin\theta_0}{z+R(1-\sin\theta_0)}\right]. \quad (14b)$$

We note that the apex term presents an additional logarithmic dependence, compared to the simpler previous expressions (Eq. (6a)); however, this result is analytical and does not require additional approximations. The cone term turns out to be similar to the one of Hudlet (Eq. (6b)), the only difference being the prefactor value.

After addition of the dielectric layer correction, the expression for the frequency shift, needed to perform fitting to data, is

$$\frac{\Delta f_{\mathrm{ES}}}{V^2} = -\frac{f_0}{2k}\pi\varepsilon_0\left[\frac{R}{(z+h/\varepsilon)^2} - \frac{R[1-\sin\theta_0]}{\left[z+h/\varepsilon+R(1-\sin\theta_0)\right]^2} + \frac{1}{z+h/\varepsilon} + \frac{1/\cos\theta_0}{z+h/\varepsilon+R(1-\sin\theta_0)}\right]. \quad (15)$$

In the following, we test the limits of applicability for these four models (Eqs. (10), (12), (13), and (15)), by comparison with experimental data measured on a metal substrate and on an ultrathin dielectric film.

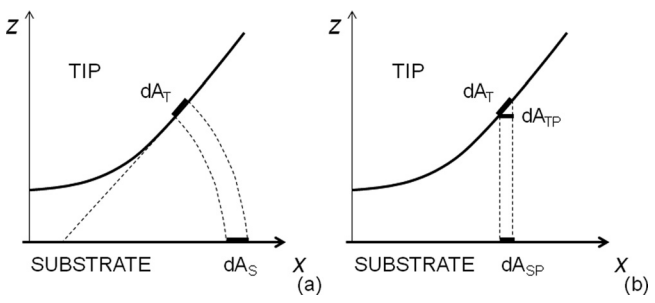

FIG. 3. (a) Dihedral approximation and (b) parallel plate approximation for the electric field lines.

EXPERIMENT

EFM and LDS measurements have been carried out using a Veeco Instruments[11] MultiMode AFM with Nanoscope IIIa controller, equipped with a Quadrex extender module for phase-locked loop (PLL) frequency-modulated operation. The Interleave mode of the Nanoscope IIIa allows alternate tapping mode profiling of the sample, with the tip/sample distance kept constant by a feedback control, and a line scan performed in "lift mode," with the same profiling repeated at a given lift height with disabled feedback control. During the lift stage, the tip is elevated from the surface by a given height, corresponding to the desired tip/sample distance, while a resonant oscillation amplitude of $A_{\mathrm{lift}} = 6\,\mathrm{nm_{pp}}$ is used to allow force gradient detection complying with Eq. (5). An alternating voltage $V(t) = V_0\cos(\Omega t)$ at frequency $\Omega/2\pi$ (30 Hz in our case) is applied to the conductive tip, with the metallic substrate connected to ground. LDS measurements herein were taken at a fixed position of the surface, by setting the lateral scanning size of the AFM to zero.

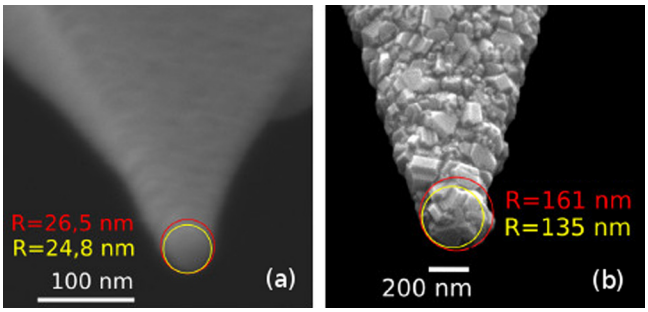

FIG. 4. SEM images of (a) small radius tip, R25; (b) large radius tip, R150. Graphical estimates of the minimum and maximum tip radii are shown.

The voltage dependent force gradient produces a resonance frequency shift, Δf (Eq. (5)), that is measured by the PLL module during the lift stage. Coherent lock-in demodulation of such frequency shift oscillation is performed at the second harmonic 2Ω, to avoid influence of any contact potential difference between the tip and sample materials,[15] using a double-phase lock-in amplifier. The frequency shift data reported in the following correspond to the RMS amplitude of the frequency shift oscillation at 2Ω, induced by the applied sinusoidal voltage. Such a measurement is proportional to the second derivative of tip/sample capacitance d^2C/dz^2. Each data point, corresponding to a different tip/sample distance, is pre-run by approaching the surface in distance-feedback conditions, by employing the lift mode, so that the effect of possible drift of the tip or sample position is reduced during data acquisition. All measurements were performed in a low humidity environment (<4% RH) by means of a sealed enclosure with desiccant and by flowing dry nitrogen gas; the temperature was stabilized to $T = 25\,^{\circ}\mathrm{C}$.

Polymer films are prepared on a metallic substrate obtained by thermal evaporation of 30 nm of gold on top of an adhesion layer of chromium (5 nm thick) previously evaporated onto a glass slide. The poly(vinyl acetate) (PVAc) had a molecular weight of 150 kg/mol and a bulk glass temperature of 37 °C. The ultrathin film had an average thickness $h = 22$ nm, obtained by spin-coating a 1% w/w solution of the polymer in toluene. The sample was annealed at $T = T_g + 20\,^{\circ}\mathrm{C}$ (were T_g is the glass transition temperature) under moderate vacuum for one day to remove residual solvent. The thickness of the PVAc film was measured using AFM profiling of a scratch on the film, produced to expose the substrate.

AFM probes of two different kinds were used in our experiments. The first ("R25") was metal-coated and had a nominal apex radius 25 nm (NanoWorld EFM50, PtIr coated), with nominal spring constant k ranging from 1.2 to 5.5 N/m, and resonance frequency in the range of 60–90 kHz. The second ("R150") was a conductive carbon probe of nominal apex radius 150 nm (AppNano, DD-ACTA, amorphous carbon coated), with nominal spring constant k in the range from 25 to 75 N/m and resonance frequency from 200 to 400 kHz. To verify their geometry and obtain reference values of apex radius and cone angle, both probes were imaged by SEM (Fig. 4). Cantilever spring constants were measured using the thermal noise method[28] implemented in a Bruker DimensionIcon-PT AFM with Nanoscope V controller. The measured values of R, θ_0, and k are reported in Table I, along with the measurement uncertainties. The resonant frequencies were determined to be 73.1 and 434.4 kHz, respectively.

RESULTS

The four analytical models (Eqs. (10), (12), (13), and (15)) are compared by acquiring force gradient vs. distance curves and by fitting the analytical expressions to these data. The comparison was performed over a broad range of tip dimensions and tip/substrate distance because of the very different apex radii, 25 nm and 150 nm, of the used tips, and by taking the force gradient vs. distance curves over distances to about 400 nm, corresponding to several tip radii.

Functions used for the fitting procedures were as follows. To improve the applicability of the model of Gomila, it was necessary to introduce an additional fitting parameter c_G, summed to $\Delta f_G/V^2$ in Eq. (10), to take into account the contribution to Δf due to the part of the tip farther away from

TABLE I. Fit parameters for $\Delta f/V^2$ with the four models in the range $0 < z < 400$ nm. (Modified Gomila's model for R25 tip was obtained on the smaller range ($0 < z < 50$ nm). The fit errors were unreasonably high and thus not reported.) All k values were obtained by constraining the result to lie within ±10% of the measured value. For Gomila's model, the value of θ_0 was also constrained within the range from 0.1 to 0.6 to obtain a reasonable fit (subscript a).

Tip	Model	R (nm)	k (N/m)	θ (rad)	c_G (Hz/V^2)	h_1 (nm)
R25	Gomila ($0 < z < 50$ nm)	50	3.1	0.1[a]	0.4	9
	Hudlet	13 ± 20	2.5 ± 7	0.7 ± 0.5	…	-1.4 ± 2
	Colchero	18 ± 2	2.5 ± 0.6	0.12 ± 0.16	…	1 ± 1
	Straight	35 ± 2	2.5 ± 0.3	0.61 ± 0.03	…	4 ± 1
	Measured	25 ± 3[b]	2.8 ± 0.3[c]	0.31 ± 0.06[b]	…	…
R150	Gomila	220 ± 130	71.5 ± 40	0.1 ± 0.6[a]	$(19 \pm 1)10^{-3}$	16.12 ± 0.01
	Hudlet	200 ± 90	71.5 ± 40	0.6 ± 0.1	…	14 ± 1
	Colchero	190 ± 90	71.5 ± 36	0.12 ± 0.30	…	13 ± 1
	Straight	250 ± 50	71.5 ± 20	0.63 ± 0.05	…	17 ± 1
	Measured	150 ± 20[b]	65 ± 6.5[c]	0.33 ± 0.05[b]	…	…

[a]Constrained from 0.1 to 0.6
[b]Obtained by SEM imaging
[c]Obtained by thermal noise calibration

the sample. Indeed, before introducing this parameter, no reliable fitting was possible using Gomila's model (data not shown). Since the force gradient has a steeper distance dependence than that of the force, c_G can be considered as a first approximation for the cone contribution at small distance values. Indeed, by comparison to the three extended models in the case of $z + h/\varepsilon \ll R(1 - \sin\theta_0)$, the functional form of c_G can be obtained. For instance, in the case of Hudlet's model

$$c_{GH} \approx -\frac{f_0}{2k}\frac{\pi\varepsilon_0 \sin\theta_0(1+2\sin\theta_0)}{(\pi/2-\theta_0)^2 R(1-\sin\theta_0)}. \quad (16)$$

A further fitting variable, h_1, had to be introduced in all models, and summed to the distance z in order to take into account any error in the tip/sample distance calibration of the AFM. In this respect, h_1 should: (i) remain the same for different samples (e.g., bare metallic substrate and substrate with dielectric film) measured with the same tip and cantilever, without altering AFM optical lever detection alignment, and (ii) be smaller than the estimated distance calibration uncertainty in our setup ($h_1 \leq 3$ nm). Concerning the fitting procedure, some of the fitting parameters can be fixed (for instance, the polymer thickness h) or constrained to improve fitting stability. In fitting to data measured on polymer films, all parameters except ε are fixed to the values previously used for fitting to bare substrate data.[29] In the following, for the sake of brevity a detailed analysis of the fit results will be carried out comparing Gomila's model (Eq. (10)) and only one of the extended models, namely, Hudlet's one (Eq. (12)). In the summary tables and the discussion, results for all four models are presented.

Figs. 5(a) and 5(b) show the resonance frequency shift RMS amplitude divided by the square of the applied voltage, $\Delta f/V^2$ (solid points), as a function of the distance from the substrate, for the case of the metallic substrate without dielectric layer ($h = 0$), using the probe R25. The solid lines in Fig. 5(a) are the two fits of the modified Gomila model. In Fig. 5(a), two fits are reported, the first obtained only by fitting to the data at small z (range of 0–50 nm), and the second for a larger z range (0–350 nm). In both cases, h was set to 0, meaning an absence of polymer film, and the parameter k was allowed to vary only within the error determined by the thermal noise method ($2.5 \leq k \leq 3.1$ N/m); this decreases the uncertainty of the fit parameters. We found that the modified Gomila model was not able to describe accurately the behavior of $\Delta f/V^2$ over the entire range of distances for probe R25, with a clear deviation from the data observed. The best fitting parameters obtained in the small range of distance ($0 < z < 50\,\text{nm} \approx 2R$), where the fit curve gives a reasonable interpolation of data at least for the smaller distance values, are listed in Table I.

The geometrical dimensions of the probe obtained from the fit procedure for the smaller tip (R25) do not agree with those measured directly by SEM (Table I). For example, the apex radius obtained by fitting with the modified Gomila model is twice that measured by SEM for probe R25. Moreover, the z-calibration correction term h_1 was higher than the known uncertainty.

A second set of measurements was taken with the larger tip (R150) (Figures 6(a) and 6(b)). In this case, the modified Gomila model described well the frequency shift data (Figure 6(a)); moreover, the values of geometrical parameters from the fitting agree with the experimental values within the error, although they have a large uncertainty (Table I). Such uncertainty depends *inter alia* on the correlation among some of the fitting parameters; by fixing some of them during the analysis procedure the error could be substantially reduced. However, the latter procedure requires the knowledge of the correct values of the parameters, and therefore was not adopted.

For a small enough tip/sample distance, the behavior of $\Delta f/V^2$ vs distance can be reduced to a single power law dependence. This simple model was adopted in the literature, especially when dealing with 3D objects such as nanoparticles.[30,31] However, our attempts to use such simplifications were unsuccessful for the larger distance range. As an example, a power law fitting of data is reported in Figs. 5(a) and 6(a), where discrepancy is obvious for the case of the smaller tip. We stress that the focus of the present work is instead to improve the description of data in the broader distance interval.

Figures 5(b) and 6(b) show the test of the extended Hudlet model (Eq. (12)) for the description of the frequency shift obtained with both probes. We note that for the extended model it was not necessary to add the constant c_G, thus reducing the available adjustable parameters by one

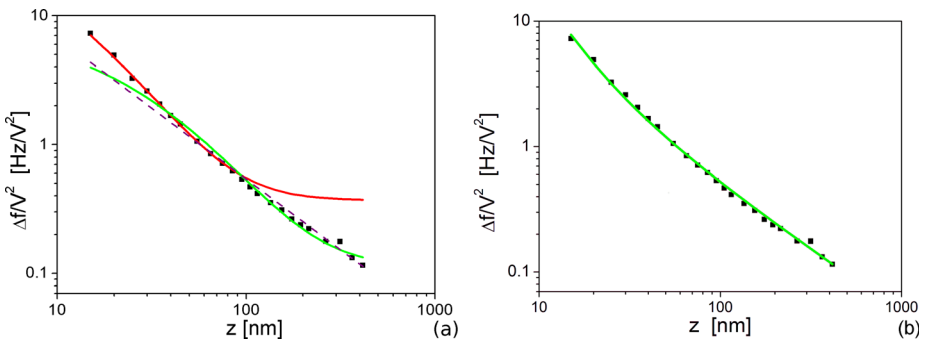

FIG. 5. Frequency shift oscillation amplitude divided by the square of the applied voltage as a function of tip/substrate distance for bare substrate ($h = 0$) with the tip R25. (a) Fitting with Gomila's model (Eq. (10)) modified by the sum of a constant. Red: fitting curve on the reduced distance range (up to 50 nm); Green: fitting curve on the extended distance range (up to 400 nm). A single power law fitting is also shown (dashed line). The value of the fitting exponent is -1.10 ± 0.03. (b) Fitting with extended model (Eq. (12)) on the full distance range. Best fit parameters are listed in Table I.

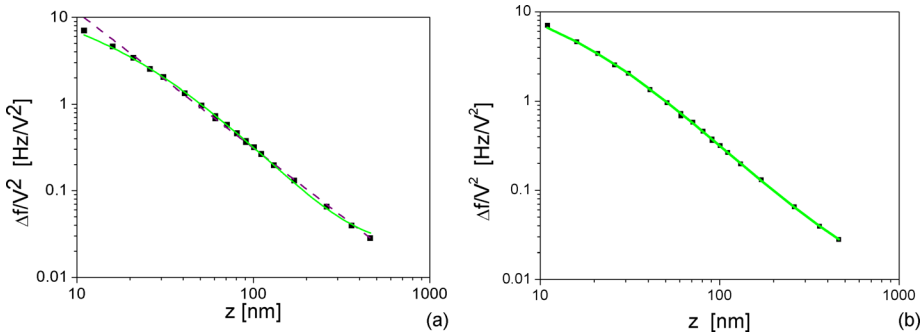

FIG. 6. Same of Fig. 5, but with the R150 tip. The value of the exponent of single power law fitting shown in (a) by the dashed line is -1.57 ± 0.02.

from the modified Gomila model. As shown in Figures 5(b) and 6(b), the extended model described well the data over the entire range for both the small (R25) and large (R150) probes. Moreover, the best fit parameters (Table I) are in reasonable agreement with the actual dimensions of the probes. To decrease the uncertainty of the fitting procedure, the parameter k was only allowed to vary within the error of its experimental determination. Thus, notwithstanding the reduced number of parameters, the extended model (Eq. (12)) gives a better description of the data than the modified Gomila model, and yields more reasonable values for the probe dimensions. Similar results were found also for the other two extended models (Eqs. (13) and (15)), the parameters for which are reported in Table I (figures not shown).

After geometrical parameters of the two probes were determined from measurements on the metallic substrate, the probes were used to measure frequency shift data on a 22 nm PVAc film (Figures 7 and 8). The equations were used to interpolate the data, with only one adjustable parameter, the dielectric constant of the film, ε; the other parameters were fixed at the values previously determined for the bare substrate (Table I), and using the measured film thickness h. The values of ε determined using the EFM with the four different models are given in Table II.

DISCUSSION

Notwithstanding the addition of the constant term c_G, the modified Gomila model gives a good description of the data over a z-range up to 1–2 times R; that is, over the entire z-range for the larger probe ($R \approx 150$ nm) and over the range of 0–50 nm for the smaller one ($R \approx 25$ nm). On the other hand, the extended models give a good description of the data for both probes over the entire range of distances, as expected since the introduction of the cone contribution extends the range of applicability of the force models, even though this reduces the number of free parameters compared to the modified Gomila model. The goal of this work was to assess the different models for their ability to estimate the ε of ultrathin polymer films. The values of ε determined by the four different models are listed in Table II. To verify their accuracy, we can compare the values with the dielectric constant measured in the bulk using conventional dielectric spectroscopy on the same material, or that estimated in ultrathin films in Ref. 13. The former is 3.4 ± 0.3 ($T = 31\,^{\circ}\mathrm{C}$ and frequency of 30 Hz) and the latter 2.9 ± 0.3 ($T = 22\,^{\circ}\mathrm{C}$ and d.c. measurement).

Considering measurements with the R25 probe, all the models evaluated herein give satisfactory results in the $0 < z \leq 50$ nm range. The obtained values of ε are in the range of 2.9–3.0, in agreement with the known value within the experimental error (Table II). Thus, these models give comparable values of ε when tested for a smaller range of distances, $z \leq 2R$, although the Gomila model (Eq. (10)) requires an additional fitting parameter (c_G). Over the entire range of distances, up to 400 nm, there is a trend towards the bulk value for the modified Gomila model (only the apex term), the Hudlet model (same apex and cone term integrated on tip), the Colchero model (same apex and cone term integrated on surface), and the Straight model.

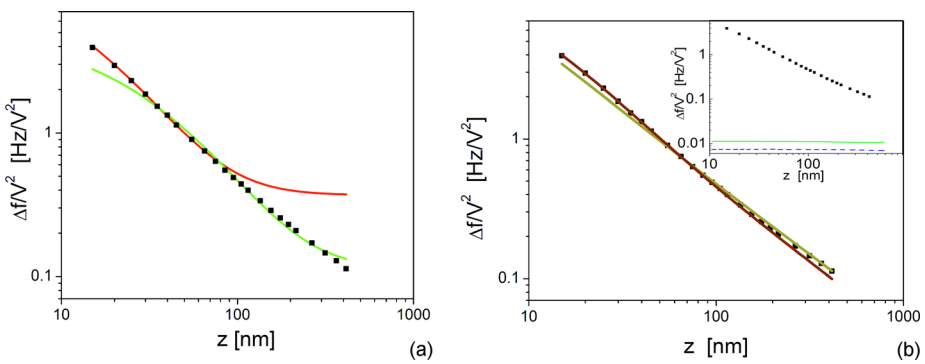

FIG. 7. Frequency shift oscillation amplitude divided by the square of the applied voltage as a function of tip/sample distance for R25 tip and 22-nm PVAc layer on metal substrate. (a) Fitting with modified Gomila's model. Red: fitting over reduced range (up to 50 nm); Green: fitting over the extended range (up to 400 nm). (b) Fitting with extended model (Eq. (12)). Red: fitting over the reduced range (up to 50 nm); Green: fitting over the extended range (up to 400 nm). The fit parameters are listed in Table II. In the inset to panel (b), the contribution from the cantilever as calculated from the equation in Ref. 19 (blue dashed line) and the equation in Ref. 27 (green solid line) is shown for comparison.

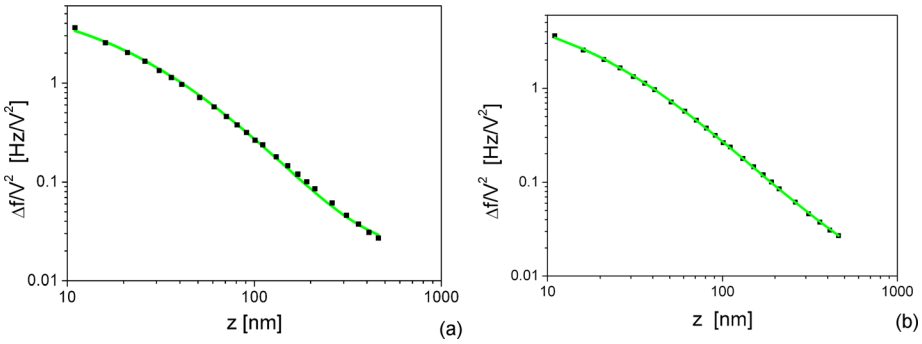

FIG. 8. Frequency shift oscillation amplitude divided by the square of the applied voltage as a function of tip/sample distance for R150 tip and 22-nm PVAc layer on metal substrate. (a) Fitting with modified Gomila's model. (b) Fitting with extended model (Eq. (12)). Fit parameters are listed in Table II.

TABLE II. Values of the dielectric constant obtained by the different models for different tip-sample distance ranges. For the R25 tip fitted by the modified Gomila's model, only the result for $0 < z < 50$ nm is reported, since for the larger range fitting results were not meaningful.

Probe	Range (nm)	ε (Gomila's model)	ε (Hudlet extended model)	ε (Colchero extended model)	ε (Straight extended model)
R25	0–400	…	2.5 ± 0.1	2.7 ± 0.1	2.8 ± 0.1
R25	0–50	3.0 ± 0.1	2.9 ± 0.1	2.9 ± 0.1	2.9 ± 0.1
R150	0–400	2.3 ± 0.1	2.2 ± 0.1	2.3 ± 0.1	2.3 ± 0.1

The equivalence of the results from Gomila model and the extended models is expected when tip/sample distances of the order of R are considered. Indeed, the Hudlet extended model is *de facto* an extension of Gomila's for larger $(z + h/\varepsilon)/R$ ratios. The results presented herein confirm such an extension for a distance up to more than $10R$. The Hudlet model underestimates the tip/sample force in comparison to the Colchero and Straight models, as seen, for example, by comparing the cone contributions, Eqs. (6b) and (7).[32] Consequently, the value of ε, which is proportional to the polarization charges on the sample interacting with the tip, is smaller when estimated using the Hudlet model.

For measurements carried out with the larger apex radius probe (R150), all models give a good qualitative description of the frequency shift over the whole range of distances, for both the polymer and the bare substrate (Figures 6 and 8); they also provide equivalent values of ε within the experimental error. We notice, however, that the found values of ε are significantly smaller than expected. This discrepancy could be due to the more irregular geometry of the larger tip, as visible by SEM imaging (Fig. 4), thus deviating from the assumed spherical shape. Such irregularity cannot be described accurately using the present analytical models, thus introducing deviation from the description of the electrostatic interactions.

Finally, we remark that the contribution from the cantilever to the force gradient is not included in any of the considered expressions. In fact, this contribution is generally calculated to be smaller than that from the cone, becoming significant only at larger distances than those considered herein. Plotted in the inset of Fig. 7(b) is the cantilever contribution calculated from the models proposed by Colchero *et al.*[19] and Miccio *et al.*[27] In the former case, the polymer contribution has been introduced by replacing z with $z + h/\varepsilon$; in the second case, it was included in the original derivation. The calculation was carried out for a 20 nm dielectric film with $\varepsilon = 4.6–1.01i$, and for a cantilever with $k = 2.8$ N/m, resonance frequency 70 kHz, length $l = 225\ \mu$m, width $28\ \mu$m, and cone height $H = 15\ \mu$m. We notice that the two approaches give comparable predictions for the cantilever contribution that from Ref. 27 being larger by about a factor 2 than that from Ref. 19. In both cases, it appears that the contribution is negligible in the range of distance herein considered.

CONCLUSION

Electric force vs distance curves for a 22 nm thick PVAc film, measured by EFM using two AFM probes with different radius, were analyzed by application of four different models, with the dielectric constant calculated. None of the considered models provide a satisfactory estimation of ε from data measured using the carbon coated, larger radius probe; the obtained value is about 25% too small. This underestimate is ascribed to the fact that the irregularities introduced by the carbon coating (evident in the SEM image of the tip of Fig. 4(b)) are not represented by a model considering a spherical apex joined to a truncated cone. We also conclude that, as expected, the equation proposed by Gomila is accurate for the smaller probe only for tip/sample distances less than $2R$, although to obtain reasonable fits an empirical constant term (C_G) must be added to the frequency shift. In order to improve the fits to larger distances, the model must include a contribution from the force acting on the cone, rather than considering only the apex. Note that adding the cone contribution to the forces, and consequently to the frequency shifts, reduces the number of free parameters available in fitting the model to experimental data. In fact, the constant term added to the apex contribution of the Gomila equation is replaced by an expression for the cone contribution that depends on the same parameter set than the apex. Consequently, the extended models can describe data over larger distances with one less free parameter. The three extended models gave qualitatively good interpolation of the experimental curves for the smaller tip radius over the full range considered herein up to $z/R \approx 15$. Regarding

quantitative estimation of ε, we note that the modified Gomila equation gives similar values compared to the other three models, when data are considered over a distance range $z/R < 2$, while no fitting is possible whatsoever when the distance range is extended. Therefore, the proposed extended models, taking into account the contribution of the cone, enable high spatial resolution with accurate quantitative results for tips with very small R, without the necessity of restricting measurements to extremely short tip/sample distances.

ACKNOWLEDGMENTS

We thank Pasqualantonio Pingue (Laboratorio NEST, Scuola Normale Superiore) for SEM imaging of AFM tips and spring constant calibration of cantilevers, Fabio Zulli (University of Pisa) for help with spin-coating depositions, and Marco Bianucci (University of Pisa) for technical assistance. This study has been partially supported by Italian Foreign Affairs Ministry—DGPSP within the Executive Programme for Scientific and Technological Cooperation between the Italian Republic and the People's Republic of China 2013-2015 (Significant Research Project No. PGR00137). The work at NRL was supported by the Office of Naval Research, in part by Code 332.

[1]G. Cao and Y. Wang, *Nanostructures and Nanomaterials: Synthesis, Properties and Applications*, 2nd ed. (World Scientific Publishing, Singapore, 2011).
[2]J. I. Sohn, Y.-S. Kim, C. Nam, B. K. Cho, T.-Y. Seong, and S. Lee, "Fabrication of high-density arrays of individually isolated nanocapacitors using anodic aluminum oxide templates and carbon nanotubes," Appl. Phys. Lett. **87**, 123115 (2005).
[3]Y. Martin, D. W. Abraham, and H. K. Wickramasinghe, "High resolution capacitance measurement and potentiometry by force microscopy," Appl. Phys. Lett. **52**, 1103 (1988).
[4]M. Labardi, D. Prevosto, K. H. Nguyen, S. Capaccioli, M. Lucchesi, and P. A. Rolla, "Local dielectric spectroscopy of nanocomposite materials interfaces," J. Vac. Sci. Technol., B **28**(3), C4D11 (2010).
[5]U. Zerweck, C. Loppacher, T. Otto, S. Grafström, and L. M. Eng, "Accuracy and resolution limits of Kelvin probe force microscopy," Phys. Rev. B **71**, 125424 (2005).
[6]P. De Wolf, T. Clarysse, W. Vandervorst, L. Hellemans, Ph. Niedermann, and W. Hanni, "Cross-sectional nano-spreading resistance profiling," J. Vac. Sci. Technol., B **16**, 355 (1998).
[7]M. Lucchesi, G. Privitera, M. Labardi, D. Prevosto, S. Capaccioli, and P. Pingue, "Electrostatic force microscopy and potentiometry of realistic nanostructured systems," J. Appl. Phys. **105**, 054301 (2009).
[8]L. Fumagalli, G. Ferrari, M. Sampietro, and G. Gomila, "Dielectric-constant measurement of thin insulating films at low frequency by nanoscale capacitance microscopy," Appl. Phys. Lett. **91**, 243110 (2007).
[9]G. M. Sacha, E. Sahagún, and J. J. Sáenz, "A method for calculating capacitances and electrostatic forces in atomic force microscopy," J. Appl. Phys. **101**, 024310 (2007).
[10]G. Gomila, J. Toset, and L. Fumagalli, "Nanoscale capacitance microscopy of thin dielectric films," J. Appl. Phys. **104**, 024315 (2008).
[11]Veeco Instruments, Sunnyvale (CA), USA.
[12]G. Gramse, G. Gomila, and L. Fumagalli, "Quantifying the dielectric constant of thick insulators by electrostatic force microscopy: Effects of the microscopic parts of the probe," Nanotechnology **23**, 205703 (2012).
[13]C. Riedel, R. Arinero, P. Tordjeman, M. Ramonda, G. Leveque, G. A. Schwartz, D. G. De Oteyza, A. Alegría, and J. Colmenero, "Determination of the nanoscale dielectric constant by means of a double pass method using electrostatic force microscopy," J. Appl. Phys. **106**, 024315 (2009).
[14]P. S. Crider, M. R. Majewski, J. Zhang, H. Oukris, and N. E. Israeloff, "Local dielectric spectroscopy of polymer films," Appl. Phys. Lett. **91**, 013102 (2007).
[15]H. K. Nguyen, D. Prevosto, M. Labardi, S. Capaccioli, M. Lucchesi, and P. A. Rolla, "Effect of confinement on structural relaxation in ultrathin polymer films investigated by local dielectric spectroscopy," Macromolecules **44**, 6588 (2011).
[16]K. Androulaki, K. Chrissopoulou, D. Prevosto, M. Labardi, and S. H. Anastasiadis, "Dynamics of hyperbranched polymers under confinement: A dielectric relaxation study," ACS Appl. Mater. Interfaces **7**, 12387 (2015).
[17]*Broadband Dielectric Spectroscopy*, edited by F. Kremer and A. Schönhals (Springer-Verlag, Heidelberg, 2003).
[18]Y. Martin, C. C. Williams, and H. K. Wickramasinghe, "Atomic force microscope: Force mapping and profiling on a sub 100 angstrom scale," J. Appl. Phys. **61**, 4723 (1987).
[19]J. Colchero, A. Gil, and A. M. Baró, "Resolution enhancement and improved data interpretation in electrostatic force microscopy," Phys. Rev. B **64**, 245403 (2001).
[20]M. Labardi, S. Patanè, and M. Allegrini, "Artifact-free near-field optical imaging by apertureless microscopy," Appl. Phys. Lett. **77**, 621 (2000).
[21]R. Hillenbrand and F. Keilmann, "Complex optical constants on a subwavelength scale," Phys. Rev. Lett. **85**, 3029 (2000).
[22]M. Labardi, J. H. Park, H. K. Nguyen, D. Prevosto, C.-Y. Seong, A. Mrzel, and G. Scalia, "Local dielectric spectroscopy of polyvinylpyrrolidone–$Mo_6S_2I_8$ nanowire composite," J. Non-Cryst. Solids **379**, 224 (2013).
[23]R. Casalini, D. Prevosto, M. Labardi, and C. M. Roland, "Effect of interface interaction on the segmental dynamics of poly(vinylacetate) investigated by local dielectric spectroscopy," ACS Macro Lett. **4**, 1022 (2015).
[24]S. Hudlet, M. Saint Jean, C. Guthman, and J. Berger, "Evaluation of the capacitive force between an atomic force microscopy tip and a metallic surface," Eur. Phys. J. B **2**, 5 (1998).
[25]In Ref. 24, a typo in the expression for $F_{\text{total}} = F_{\text{apex}} + F_{\text{cone}}$ after Eq. (9) therein is here corrected (see also Ref. 26). Furthermore, the prefactor of the expression for F_{cone} before Eq. (7) is used by us, instead than the more refined one included in Eq. (9), to allow better comparison with other literature.
[26]B. M. Law and F. Rieutord, "Electrostatic forces in atomic force microscopy," Phys. Rev. B **66**, 035402 (2002).
[27]L. A. Miccio, M. M. Kummali, G. A. Schwartz, A. Alegria, and J. Colmenero, "Dielectric spectroscopy at the nanoscale by atomic force microscopy: A simple model linking materials properties and experimental response," J. Appl. Phys. **115**, 184305 (2014).
[28]J. L. Hutter and J. Bechhoefer, "Calibration of atomic-force microscope," Tips. Rev. Sci. Instrum. **64**, 1868 (1993).
[29]In fitting dielectric spectra $\varepsilon(\Omega)$, z becomes a constant and the excitation frequency Ω becomes the independent variable. The latter point will be the subject of a further work.
[30]T. D. Krauss and L. E. Brus, "Charge, polarizability, and photoionization of single semiconductor nanocrystals," Phys. Rev. Lett. **83**, 4840 (1999).
[31]T. Melin, H. Diesinger, D. Deresmes, and D. Stievenard, "Electric force microscopy of individually charged nanoparticles on conductors: an analytical model for quantitative charge imaging," Phys. Rev. B **69**, 035321 (2004).
[32]This is a consequence of the assumption of constant field along the (assumed) circular field line together with the calculation of the force acting on the charges at the tip surface instead of at the film surface.